ON THE ANALYSIS OF DISPERSION RELATION OF SPATIALLY SHOALING WAVES

David W. Wang, James M. Kaihatu and Paul A. Hwang

Oceanography Division, Naval Research Laboratory,
Stennis Space Center, MS 39529

1. INTRODUCTION

As waves propagate into nearshore waters, the wave dispersive relation is significantly affected by the nonlinear dynamics of the shoaling process (Herbers et al. 2002). This could have important effects to the interpretation and application of remote sensing results of shallow water waves (Stockdon and Holman, 2000). Many field studies are carried out based on temporally measured wave data to examine and clarify the wave dispersion relation in shallow waters (Thornton and Guza, 1982; Herber et al. 2002). Recently, an airborne topographic mapper (ATM, an airborne scanning laser ranging system) has bee n deployed to acquire three-dimensional (3D) topography of ocean surface waves off the coast of Duck, North Carolina (Hwang et al. 2000). The ATM spatial wave data reveal the typical shoaling wave features of a decreasing wavelength and skewed wave profile with a shaper crest and flatter trough. These shoaling features occur within a short distance relative to wave length. Analyzing the dispersion relation of the spatially shoaling waves requires methods that can deal with these non-stationary and nonlinear features. In this study, we explore the application of the Fourier-based wavelet analysis to examine the dispersion relation.

2. WAVELET CROSS SPECTRUM METHOD

Applying the Morlet-based wavelet transformation (Liu, 2000) to two space series of surface wave elevation, $\eta_1(x)$ and $\eta_2(x)$, along a transect direction measured at times t_1 and t_2, the cross spectrum of the two space series is derived. The phase difference between the two space series can be computed from the co- and quad-spectrum of the cross spectrum, expressed as C_{12} and Q_{12} in wavenumber-space domain, respectively,

$$\triangle\phi_{12}(k,x) = \tan^{-1}\left(\frac{Q_{12}(k,x)}{C_{12}(k,x)}\right). \tag{1}$$

The local wave frequency in wavenumber-space domain can then be computed from

$$\omega_{12}(k,x) = \frac{\phi_{12}(k,x)}{\Delta t}, \tag{2}$$

where Δt is the time lag between the two space series ($\Delta t = t_2 - t_1$). This local wave frequency from the cross spectrum analysis of two space series is very similar to the derivation of wavenumber from time series at two adjacent wave gauges in many studies (e.g. Thronton and Guza, 1982; Donelan et al. 1996). The local wave phase speed in wavenumber-space domain can be computed as

$$C(k,x) = \frac{\omega(k,x)}{k} \tag{3}$$

3. DATA ANALYSIS RESULTS

3.1 Simulated monochromatic waves

We first applied the wavelet method to numerically simulated shoaling waves. The shoaling wave data are generated by a frequency domain parabolic mild-slope model with and without nonlinear wave-wave interaction (Kaihatu and

Kirby 1995; Kirby and Kaihatu 1996). The simulations are initialized offshore by a 10-s wave (deep water wave frequency ω_o=0.628 rad/s) with 0.2 m wave height. The simulation of shoaling waves is over a sloping bottom bathymetry with a gentle slope of 0.009. Because there no depth variations in the along-shore direction, the 2D simulated wave field is treated as 1D simulation.

Figure 1a shows two space series of linear shoaling wave profile $\eta_1(x)$ and $\eta_2(x)$ generated at a time spacing of 1s. The shoaling waves display a decreasing wavelength as water depth decreases. Also shown is the image of wavelet spectrum of $\eta_1(x)$ (Fig. 1b). The wavelet spectrum shows that the wavenumber-space wave energy distribution has most energy concentrated within a very narrow wavenumber band. The local peak wavenumber k_p from the wavelet spectrum (Fig. 1c) increases from 0.1 to 0.3 rad/m as water depth decreases from 10 to 1 m. Figure 1d shows the local peak wave frequency associated with k_p derived from (2). The local frequency remains constant and agree with ω_o=0.628 rad/s. Figure 3e show the local peak wave phase speed computed from (3) versus the relative water depth normalized by the deep water wavenumber. Also shown is the phase speed from the linear dispersion relation,

$$C_l = C_0 \tanh(kh)\,, \tag{4}$$

where h is water depth and C_o is the phase speed based on the deep water linear dispersion for wave frequency ω expressed as

$$C_0 = \frac{g}{\omega}. \tag{5}$$

The local peak wave phase speed obtained from the wavelet cross spectrum method agrees well with that from the linear dispersion relation. The larger discrepancy at deeper and shallower water is caused by the edge effect of the wavelet method.

Figure 2a shows the space series $\eta_1(x)$ and $\eta_2(x)$ of the simulated nonlinear wave field. The wave profile displays a strong nonlinear effect with increasingly sharper crests and flatter troughs as wave moves into shallower waters. The wavelet spectrum of $\eta_1(x)$ is shown in Fig 2b. In deeper water, the wave energy concentrates in a narrow wavenumber band. The peak wavenumber gradually increases as water depth decreases. As waves move into shallower waters, the wave spectrum broadens with a secondary energy peak appearing at higher wavenumbers (about twice of the primary peak wavenumber). The secondary peak become more pounced as water depth further decreases. The peak wavenumbers of the primary and secondary spectral peaks are shown in Fig. 2c. Both peak wavenumbers increase as wave moves into shallower waters. The local peak wave frequencies associated with the two wavenumber peaks derived from (2) are shown in Fig. 2d. Both the local peak wave frequencies remain relatively constant with the peak frequency of the magnitude of the secondary spectral peak about twice of the peak frequency of primary peak wave frequency. The local phase speed associated with the two peaks are computed and shown in Fig 2e. The phase speed of the secondary peak follows the phase speed of the primary peak, which decrease as water depth decrease. This implies that the secondary peak at higher wavenumbers is the bound harmonic of the free waves around the primary peak. To account for the nonlinear effect on dispersion relation in shallow water, a modified dispersion relation is proposed (Hedges, 1976; Kirby and Dalrymple, 1986),

$$C_{nl} = C_0 \tanh(kh + A)\,, \tag{6}$$

where A is the local amplitude of the wave profile. Figure 3 shows the normalized water depth versus local peak phase speed from (3) and the phase speeds by the linear and nonlinear dispersion relation from (4) and (6), respectively. The phase speed of nonlinear shoaling waves by (3) is generally between the phase speeds from the linear and nonlinear dispersion. At relatively deeper water ($k_0h > 2$), the peak phase speed agree well with that from the linear dispersion relation. As waves shoal, the phase speed becomes larger and moves closer to that by the nonlinear dispersion relation. At $k_0h < 0.7$, the phase speed of the nonlinear shoaling wave agrees well with that from the nonlinear dispersion relation (6).

The above results suggest that local wave frequency and phase speed derived by the wavelet cross spectrum method can effectively examine and reveal the underlying linear and nonlinear dispersive characteristics of shoaling waves.

3.2 ATM data

The ATM uses a nutating scanning mirror to project the laser beam in a circular pattern on the ocean surface. The front (forward) and rear (backward) halves of the circular scanning cycles produce two time-lapsed images of the surface waves. A given position over ocean surface waves scanned by the laser beam of an azimuthal angle in the front half of the scanning cycle will be scanned again at conjugate azimuthal angle during the rear half of the scanning cycle later. Gathering ATM data according to a specified pair of azimuthal and its conjugate angles, space series of ocean surface wave elevation at two separated times along a transect direction in the flight direction can be extract from ATM scanning data. The time lag is not constant across the flight track. For a typical ATM flight configuration, the time lag varies from approximately 2 s at the center of the flight track to one digitization time step (1/50000 s) at the two edges. More details about the ATM measurement system can be found in Hwang et al. (2000).

Figure 4a shows the 3D surface wave topography of shoaling waves extending 3000 m offshore, which is constructed from the forward scanning during an ATM flight off the coast of Duck, North Carolina on October 17, 1994. The wave field is dominated by easterly swells. More details about these data can be found in Hwang et al. (2000). Figure 4b is the water depth profile along the flight track. Figure 4c shows two space series of wave profile along a cross shore direction as indicated by the dashed line in Fig. 4a. This two space series $\eta_1(x)$ and $\eta_2(x)$ are, respectively, from the forward and backward scanning. The time spacing of the two data set is 1.59 sec. Figure 4d shows the wavelet spectrum of $\eta_1(x)$. Instead of wave energy concentrating in a narrow band of wavenumber as shown in the linear and nonlinear simulated shoaling waves in Figs 1 and 2, the very distinguish and dominant feature in this wavelet spectrum is the presence of several energy parcels in the wavenumber-space domain. These energy parcels directly correspond to the wave groups shown in the 1D wave profiles. The presence of wave grouping and its energy parcels in wavelet spectra have also been reported in deep water wind wave data (Donelan et al. 1996; Liu, 2000).

Figure 5a shows the 1D wave profile $\eta_1(x)$ and $\eta_2(x)$ of the wave group centered at a offshore distance of about x=1700 m with a length of 350 m. There are three consecutive large waves in the group with a crest-to-trough wave height of about 2 m and wavelength of about 80~90 m. The water depth varies slowly from about 13 m to 12 m. Figure 5b shows the wavelet spectrum corresponding to the group. The wave energy peaks at wavenumber around 0.07 rad/m. Figure 5c show the local wave frequencies at three wavenumbers around the peak wavenumber (k= 0.067, 0.072, and 0.077 rad/m) computed from (2). The local wave frequencies vary within the group. The wave frequency is larger at the front of the group and decrease toward the rear end of the group. The local phase speeds are then computed from (3) and shown in Fig. 5d. A first order correction of the Doppler shift due to the ATM flight opposite to wave direction is made. Also shown is the phase speed for k=0.072 by the linear dispersion relation, which is about 10 m/s and increases slightly toward the end of the wave group as water depth increases. The peak wave phase speed within the group is largest at front of wave group and gradually decrease toward the rear end of the group. The peak phase speed is smaller than that predicted by the linear dispersion relation (4). Very similar results are also shown in another wave group centered at x= 1200 m (see Figure 6). The spatial variation of wave phase speed within a wave group is also observed in wind wave data by Donelan et al. (1996).

The presence of wave group is a dominant and distinguish signature in ATM wave data. This variation of phase speed within wave groups is clearly shown by the analysis result using the wavelet cross spectrum method. This implies that the dispersive relation of surface waves within wave group can not be properly described by the linear or nonlinear dispersion relation of monochromatic waves. The plausible causes and implications should be investigated further.

4. SUMMARY

In this study, we apply the wavelet cross spectrum method to examine the dispersion relation of spatially shoaling waves. The method provided an estimation of local wave frequency and phase speed for a shoaling wave field that often has strong non-stationary and nonlinear features induced by decreasing water depth. The analysis of ATM wave data reveals that the presence of wave groups produces a distinguish energy parcels in the wavenumber-space wavelet spectrum. The local phase speed within the wave group shows a spatial variation, which is larger at the front of the wave group and gradually decreases toward the tail end of the group. The local phase speed within the group is generally slower than that by the linear dispersion relation. This spatially variation within wave group could have important implication and should be investigated further. It is also noted that the wavelet cross spectrum method is still a Fourier-based analysis method based on the assumption of linear superposition of wave components. Strictly

speaking Fourier-based analysis should be used for periodic and stationary processes only. Shoaling waves in rapid changing water depth is certainly neither stationary nor periodic. The outcome of this analysis could also be limited by the assumptions associated with Fourier transformation inherent in the method. More discussions about issues related to the processing techniques dealing with non-stationary and nonlinear wave data are given by Hwang et. al. (2002).

ACKNOWLEDGEMENTS

This work is supported by the Office of Naval Research, Naval Research Laboratory Program Elements N61153 and N62435, (NRL Contribution PP/7330--02-66).

REFERENCES

Donelan, M. A., W. M. Drennan, and A.K. Magnusson, 1996: Nonstainary analysis of the directional properties of propagating waves. *J. Phys. Oceanogr.*, 26, 1901-1914.

Hedges, T. S., 1976: An empirical modification to linear wave theory. *Proc. Inst. Civ. Eng.*, 61, 575-579.

Herbers, T. H. C., S. Elgar, N. A. Sarap, and R. T. Guza, 2002: Nonlinear dispersion of surface gravity waves in shallow water. *J. Phys. Oceanogr.*, 32, 1181-1193.

Hwang, P. A., W. B. Krabill, W. Wright, E. J. Walsh, and R. N. Swift, 2000: Airborne scanning lidar measurements of ocean waves. *Remote Sens. Eniron.*, **73**, 236-246.

Hwang, P. A., D. W. Wang, and J. M. Kaihatu, 2002: A comparison of the energy flux computation of shoaling waves using Hilbert and wavelet spectral analysis techniques. (this issue)

Kaihatu, J.M, and J. T. Kirby, 1995: Nonlinear transformation of waves in finite water depth. *Phys. Fluids*, **7**¸ 1903-1914.

Kirby, J. T., and R. A. Dalrymple, 1986: Am approximate model for nonlinear dispersion in monochromatic wave propagation models. *Costal Eng.*, 9, 545-561.

Kirby, J. T., and J.M. Kaihatu, 1996: Structure of frequency domain models for random wave breaking, *Proc. 25th Intl. Conf. On Coastal Eng.*, Orlando, FL, ASCE, 1144-1155.

Liu, P.C., 2000 : Wave Grouping characteristics on nearshore Great Lakes, *Ocean Eng.*, 27, 1221-1230

Stockdon, H. F. and R. A. Holman, 2000: Estimation of wave phase speed and nearshore bathymetry from video imager. *J. Geophys. Res.*, **105**, C9, 22015-22033.

Thornton, E. B. and R. T. Guza, 1982: Energy saturation and phase speeds measured on a natural beach. *J. Geophys. Res.*, **87**, C12, 9499-9508.

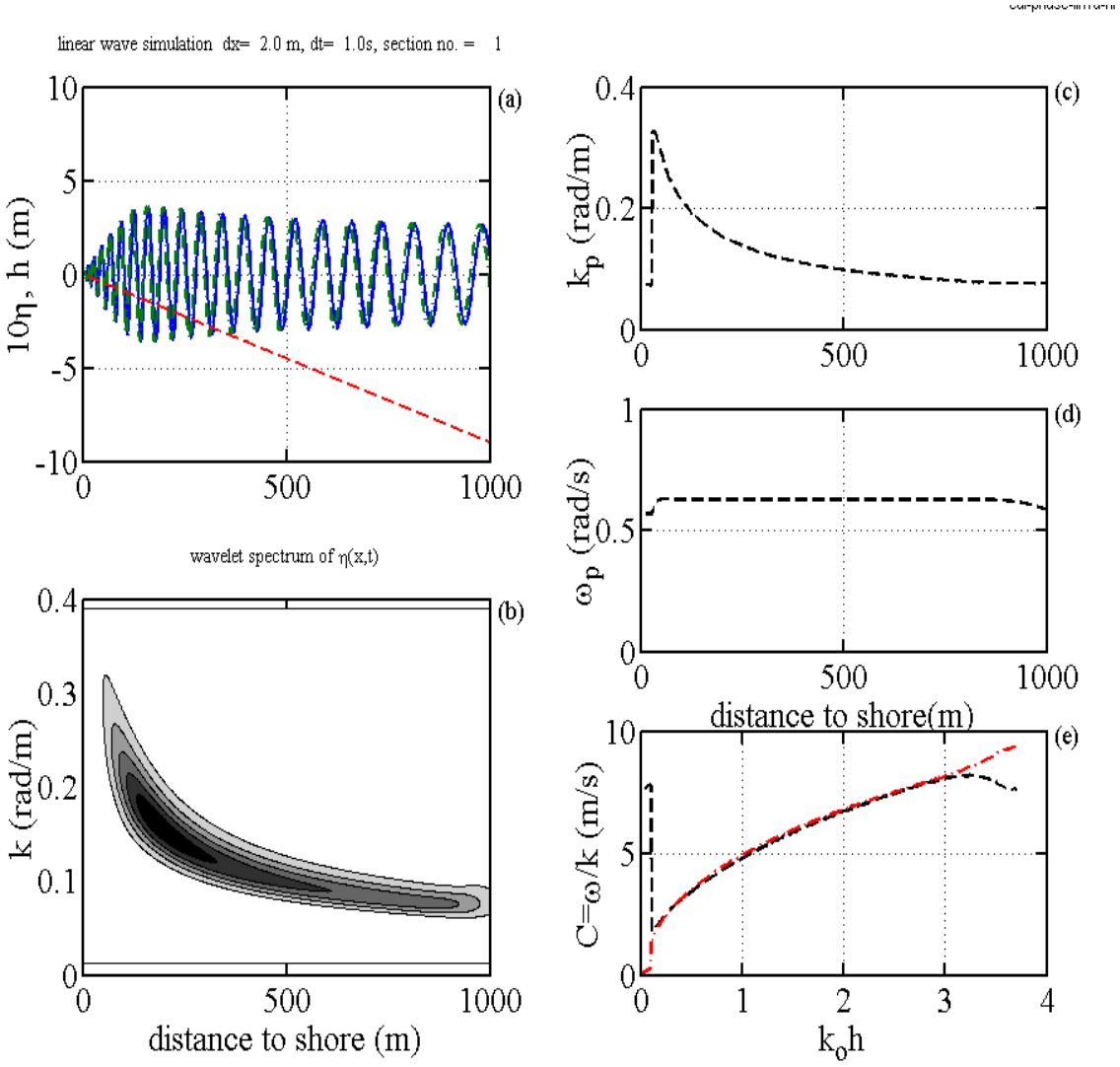

Figure 1: Analysis results of simulated linear shoaling waves (a) simulated space series of wave profiles at two time steps and the water depth profile, (b) wavelet spectrum, (c) peak wavenumber, (d) peak wave frequency, and (e) peak wave phase speed by (3) (dashed lines) and by the linear dispersion relation (dashed-dotted line)

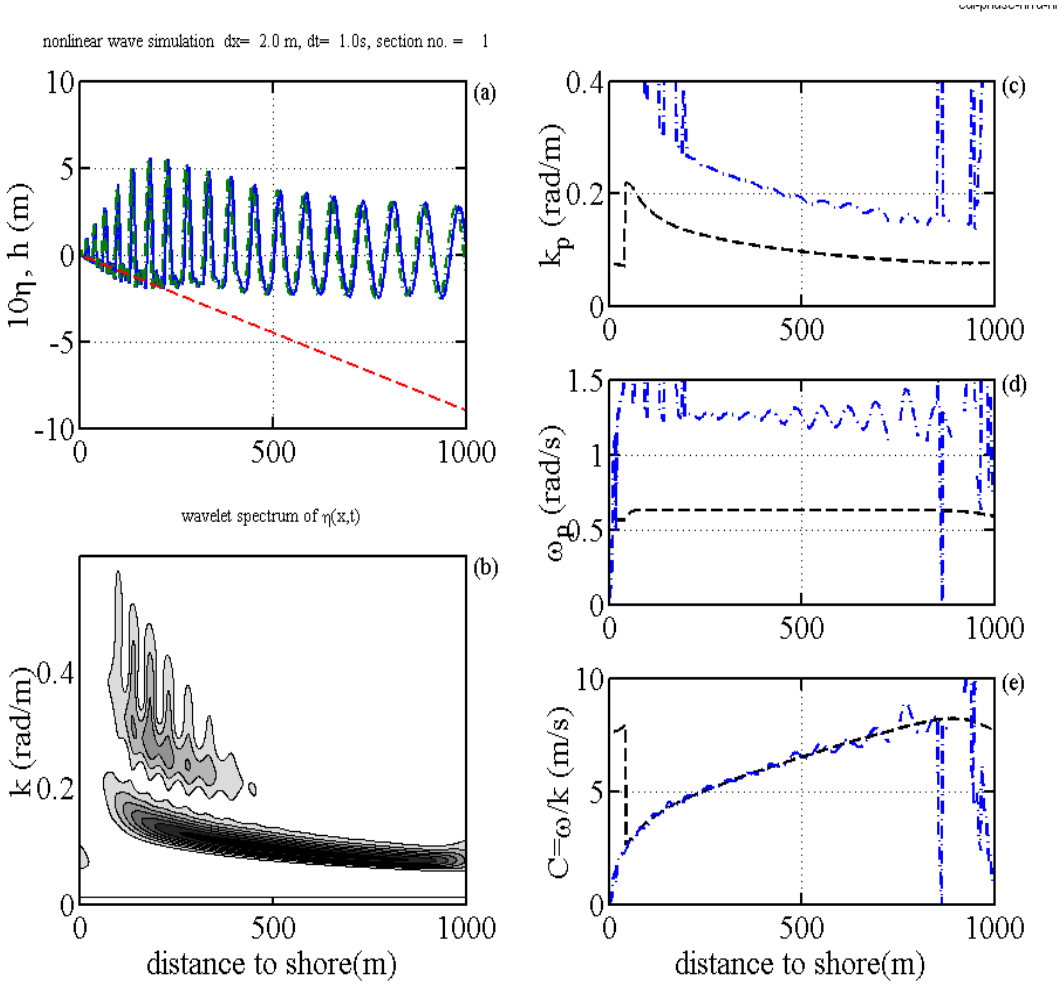

Figure 2: Same as Figure 1 but for nonlinear shoaling waves. (c), (d), and (e) primary peak (dashed line), secondary peak (dashed-dotted line)

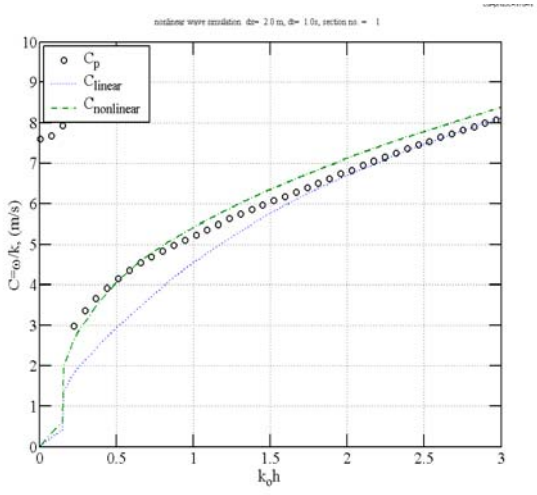

Figure 3: Phase speed versus normalized water depth, computed peak phase speed by (3) (circles), by the linear dispersion (4) (dotted line) and nonlinear dispersion (6) (dashed line).

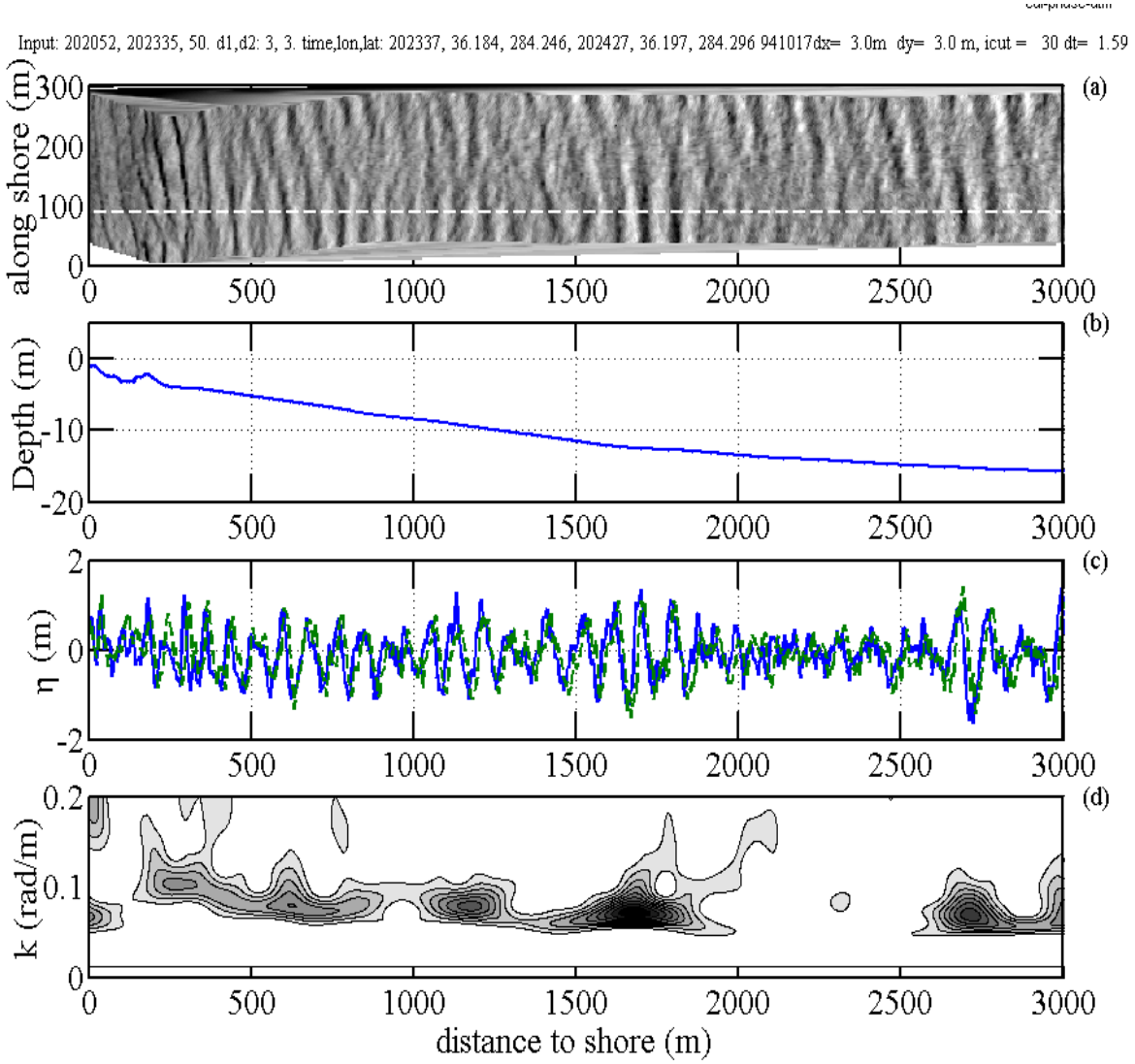

Figure 4: (a) 3D ocean surface wave topography from the ATM measurements, (b) water depth profile (c) the 1D surface wave profile along the flight direction extracted from the forward and backward scan of ATM data, (d) wavelet spectrum.

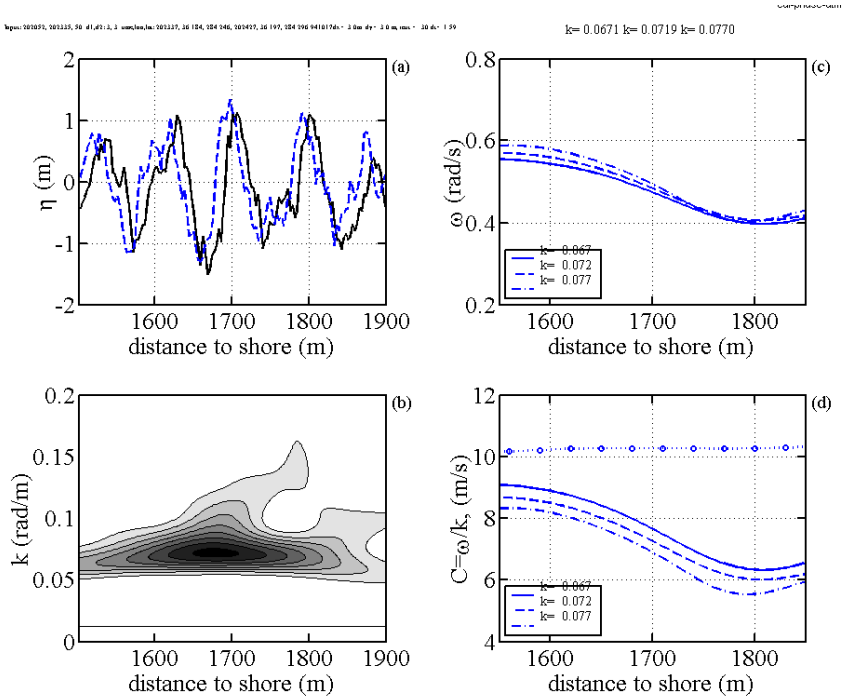

Figure 5: (a) Two 1D wave group profiles measured at time lag of 1.57 s, (b) the wavelet spectrum, (c) the local wave frequency associated with three wavenubmers around the peak wavenumber of the group, (d) local peak wave phase speed from (2) for the three wavenumbers and phase speed from the linear dispersion relation (4) for wavenumber k = 0.072 rad/m.

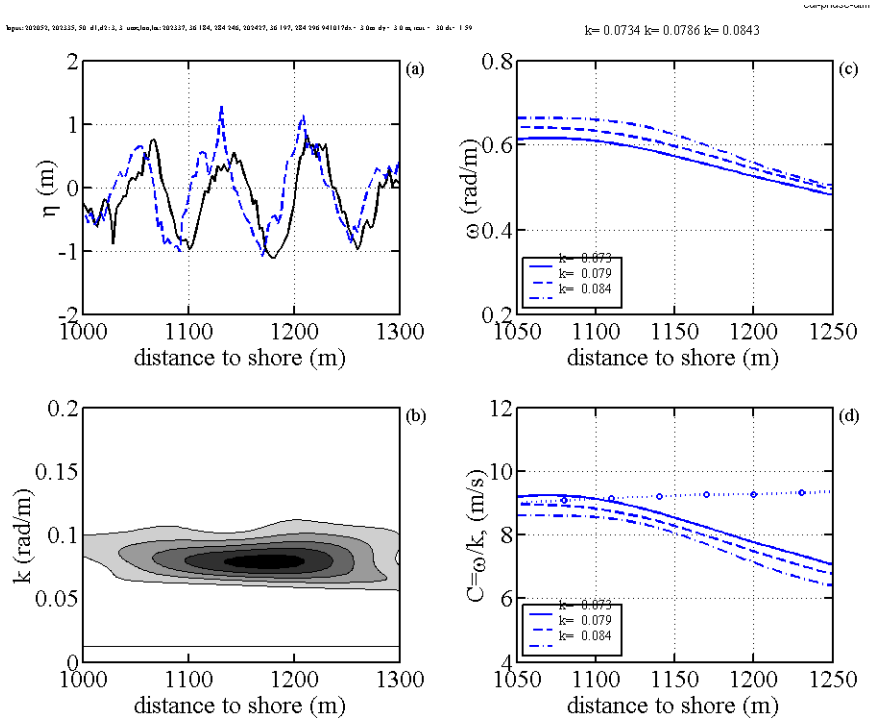

Figure 6: Same as Fig. 5 but for the wave group centered at x=1000 to 1300 m, the phase speed from the linear dispersion relation (4) is for k= 0.079 rad/m.